TU Delft

Delft University of Technology

Document Version
Final published version

Licence
CC BY

Citation (APA)
Kramer, O. J. I., de Moel, P. J., Padding, J. T., Baars, E. T., Rutten, S. B., Elarbab, A. H. E., Hooft, J. F. M., Boek, E. S., & van der Hoek, J. P. (2021). New hydraulic insights into rapid sand filter bed backwashing using the Carman–Kozeny model. *Water Research*, *197*, Article 117085. https://doi.org/10.1016/j.watres.2021.117085

Important note
To cite this publication, please use the final published version (if applicable).
Please check the document version above.

Copyright
In case the licence states “Dutch Copyright Act (Article 25fa)”, this publication was made available Green Open Access via the TU Delft Institutional Repository pursuant to Dutch Copyright Act (Article 25fa, the Taverne amendment). This provision does not affect copyright ownership.
Unless copyright is transferred by contract or statute, it remains with the copyright holder.

Sharing and reuse
Other than for strictly personal use, it is not permitted to download, forward or distribute the text or part of it, without the consent of the author(s) and/or copyright holder(s), unless the work is under an open content license such as Creative Commons.

Takedown policy
Please contact us and provide details if you believe this document breaches copyrights.
We will remove access to the work immediately and investigate your claim.

This work is downloaded from Delft University of Technology.

Water Research 197 (2021) 117085

Contents lists available at ScienceDirect

Water Research

journal homepage: www.elsevier.com/locate/watres

New hydraulic insights into rapid sand filter bed backwashing using the Carman–Kozeny model

Onno J.I. Kramer[a,b,c,d,f,*], Peter J. de Moel[a,c,e], Johan T. Padding[b], Eric T. Baars[c], Sam B. Rutten[d,g], Awad H.E. Elarbab[d], Jos F.M. Hooft[c], Edo S. Boek[f], Jan Peter van der Hoek[a,c]

[a] Delft University of Technology, Faculty of Civil Engineering and Geosciences, Department of Water Management, PO Box 5048, 2600 GA, Delft, the Netherlands
[b] Delft University of Technology, Faculty of Mechanical, Maritime and Materials Engineering, Department of Process and Energy, Leeghwaterstraat 39, 2628 CB, Delft, the Netherlands
[c] Waternet, PO Box 94370, 1090 GJ, Amsterdam, the Netherlands
[d] HU University of Applied Sciences Utrecht, Institute for Life Science and Chemistry, PO Box 12011, 3501 AA Utrecht, the Netherlands
[e] Omnisys, Eiberlaan 23, 3871 TG, Hoevelaken, the Netherlands
[f] Queen Mary University of London, Division of Chemical Engineering, School of Engineering and Materials Science, Mile End Road, London E1 4NS, United Kingdom
[g] Wetsus, European Centre of Excellence for Sustainable Water Technology, P.O. Box 1113, 8900 CC, Leeuwarden, the Netherlands

ARTICLE INFO

Article history:
Received 30 December 2020
Revised 26 February 2021
Accepted 22 March 2021
Available online 23 March 2021

Keywords:
Drinking water treatment
Multiphase flows
Filter-backwash
Hydraulics drag relations
Particle orientation
Dynamic particle shape factors

ABSTRACT

Fluid flow through a bed of solid particles is an important process that occurs in full-scale water treatment operations. The Carman–Kozeny model remains highly popular for estimating the resistance across the bed. It is common practice to use particle shape factors in fixed bed state to match the predicted drag coefficient with experimentally obtained drag coefficients. In fluidised state, however, where the same particles are considered, this particle shape factor is usually simply omitted from the model without providing appropriate reasoning. In this research, it is shown that a shape factor is not a constant particle property but is dependent on the fluid properties as well. This dynamic shape factor for irregularly shaped grains increases from approximately 0.6 to 1.0 in fluidised state.

We found that unstable packed beds in moderate up-flow conditions are pseudo-fixed and in a setting state. This results in a decreasing bed voidage and simultaneously in a decreasing drag coefficient, which seems quite contradictory. This can be explained by the collapse of local channels in the bed, leading to a more uniform flow distribution through the bed and improving the available surface for flow-through. Our experimental measurements show that the drag coefficient decreases considerably in the laminar and transition regions. This is most likely caused by particle orientation, realignment and rearrangement in particles' packing position.

A thorough hydraulic analysis shows that up-flow filtration in rapid sand filters under backwash conditions causes the particle bed to collapse almost imperceptibly. In addition, an improved expression of the drag coefficient demonstrated that the Carman–Kozeny model constant, however often assumed to be constant, is in fact not constant for increasing flow rates. Furthermore, we propose a new pseudo-3D image analysis for particles with an irregular shape. In this way, we can explain the successful method using optimisation of the extended terminal sub-fluidisation wash (ETSW) filter backwashing procedure, in which turbidity and peaks in the number of particles are reduced with a positive effect on water quality.

© 2021 The Author(s). Published by Elsevier Ltd.
This is an open access article under the CC BY license (http://creativecommons.org/licenses/by/4.0/)

1. Introduction

The downward flow of fluid through a bed of solid particles is an important process that occurs in full-scale water treatment operations (Crittenden et al., 2012). In the field of drinking wa-

* Corresponding author.
E-mail address: onno.kramer@waternet.nl (O.J.I. Kramer).

https://doi.org/10.1016/j.watres.2021.117085
0043-1354/© 2021 The Author(s). Published by Elsevier Ltd. This is an open access article under the CC BY license (http://creativecommons.org/licenses/by/4.0/)

Nomenclature

Ar	Archimedes number [-]
c_i	Coefficients [-]
D	Inner column or cylinder vessel diameter [m]
d	Measured diameter [m]
d_p	Effective or average or particle equivalent diameter [m]
$d_{s,i}$	Sieve mesh diameter [m]
f_L	Dimensionless drag coefficient (laminar representation) [-]
$f_{L,CK}$	Dimensionless drag coefficient (laminar representation for Carman–Kozeny) [-]
f_T	Dimensionless drag coefficient (turbulent representation) [-]
$f_{T,CK}$	Dimensionless drag coefficient (turbulent representation for Carman–Kozeny) [-]
g	Local gravitational field of earth equivalent to the free-fall acceleration [m/s²]
ΔL	Relative total fluid bed height [m]
L	Fluid bed height [m]
L_{mf}	Bed height at minimum fluidisation [m]
L_0	Fixed bed height [m]
N	Total number of particles / total number of experiments [#]
$\Delta P/\Delta L$	Pressure drop head loss [kPa/m]
ΔP_{max}	Total maximum differential pressure over the bed [kPa]
Q_w	Water flow [m³/h]
Re_p	Reynolds particle number [-]
Re_ϵ	Modified Reynolds particle number [-]
$Re_{\epsilon,mf}$	Modified Reynolds particle number at minimum fluidisation [-]
v_s	Linear superficial velocity or empty tube fluidisation velocity [m/s]
T	Temperature [°C]
V_p	Volume of an individual particle [m³]

Greek symbols

ε	Voidage of the system [m³/m³]
ε_0	Fixed bed voidage [-]
ε_{mf}	Voidage at minimum fluidisation [-]
η	Dynamic fluid viscosity [kg/m/s]
υ_T	Kinematic fluid viscosity [m²/s]
ϕ_s	Shape of diameter correction factor [-]
ρ_f	Fluid density [kg/m³]
ρ_p	Particle density [kg/m³]

Abbreviations

CFD	Computational Fluid Dynamics
DPI	Dots per inch
ETSW	Extended terminal sub-fluidisation wash
FTU	Formazin turbidity units
HSV	Colour model (hue, saturation, value) in graphic design
RSF	Rapid sand filtration
WHO	World Health Organisation

ter treatment, rapid sand filtration (RSF) is the most common unit operation applied to capture fine particles from the water in the filter bed. Accumulated particles cause a gradual increase in head loss and reduce overall effectiveness of the filter bed (Howe et al., 2012). When the head loss exceeds a certain threshold after a period of time, the filter is backwashed, usually assisted by some auxiliary scouring. During backwashing, an upward water flow expands the filter bed and flushes out the collected fine particles. After a filtration and backwashing sequence, the cycle starts again (Edzwald, 2011). To reduce the passage of particles through restarted filters immediately after a backwash procedure, Amburgey proposed the extended terminal sub-fluidisation wash method (ETSW) to remove significantly higher amounts of backwash remnant particles (Amburgey, 2005). ETSW is a proven method of terminating the backwash cycle with a sub-fluidisation wash for a time interval adequate to pass one theoretical filter volume of water upward through the filter (Amburgey and Amirtharajah, 2005).

ETSW is a relatively straightforward process comprising an appropriate additional sub fluidisation wash step at the end of a normal backwash procedure. The ETSW washing phase is started at the end of the backwash sequence with the purpose of rinsing out the remainder of the particles, sheared from the filter during the fluidisation stage of the backwash. The ESTW is set to a wash water flow rate below the minimum fluidisation velocity for a time sufficient to displace one entire filter volume of particle-laden water. The results presented by Amburgey (2005) show a significant improvement in water quality by reducing, or eliminating, the initial particle passage during the restart of a packed filter after backwashing. ETSW reduces the turbidity during filter maturation and particle number spikes in practice, but no hydraulic explanation for its effectiveness was provided.

In this paper, we report laboratory measurements in which upflow filtration procedures were simulated. During the experiments, an unexpected reduction in both bed voidage and bed resistance was detected which could not be explained by traditional drag coefficient correlations as a function of the particle Reynolds number. We propose this *can* be explained by differences in preferred orientation of particles under different hydraulic conditions.

2. Hydraulic drag

2.1. Hydraulic models for fluid flow in particle beds

Well-known hydraulic models for flow through particle beds have been introduced for the laminar flow regime by Blake (1922) and Kozeny (1927) based on Darcy (1856), for the turbulent flow regime by Burke and Plummer (1928), and for the transitional flow regime by Ergun (1952) and Carman (1937) based on the Forchheimer flow conditions (Forchheimer, 1930). In the laminar regime, the fluid flows in smooth parallel layers without any disturbance between the layers, while in the turbulent flow regime, the fluid undergoes irregular fluctuations and changes in both magnitude and direction. Transitional flow is a mixture of laminar and turbulent flow, with turbulence in the centre of pore spaces and laminar flow near the particle surfaces. Each of these flows behaves in different ways in terms of their frictional energy loss.

De facto, the most commonly used and most accurate (Říha et al., 2018) equation for expressing the relationship between permeability and voidage, particle size and tortuosity is the Carman–Kozeny equation. This equation is applied in various fields, such as groundwater flow, water treatment and many other water processes (Camp, 1946). The Carman–Kozeny equation is important not only for the determination of permeability in porous media (Yang, 2003), but also for the estimation of the voidage in a fluidised bed (Kramer et al., 2020a). In groundwater flow, the flow regime is generally considered to be laminar (Crittenden et al., 2012). In fluidised beds, however, not only laminar, but also transitional and, to a certain degree, turbulent flow regimes occur. The resistance of laminar flow through a granular bed can be calculated using the well-known equation proposed by Blake (1922),

Kozeny (1927) and Carman (1937):

$$\frac{\Delta P}{\Delta L} = 180 \frac{v_s \eta}{{d_p}^2} \frac{(1-\varepsilon)^2}{\varepsilon^3} \qquad (Re_\varepsilon < 2) \tag{1}$$

Where: $\Delta P/\Delta L$is the pressure drop head loss, v_s is the superficial velocity, η the dynamic fluid viscosity, d_p the average or equivalent particle diameter, ε the bed voidage and Re_ϵ the modified particle Reynolds number (Eq. (3)). This equation shows that the resistance of laminar flow is linear with the viscosity and with the superficial velocity, as is also known to be the case for laminar flow through pipes according to Hagen-Poiseuille (Munson et al., 2020) and laminar flow through aquifers (Darcy, 1856). The experimentally obtained value of 180 is often indicated as the Kozeny drag coefficient (Kozeny, 1927). Further background information about the Carman equation is elucidated in the Supplementary Material (Section 3).

Since in water treatment the operational field lies in the vicinity of incipient fluidisation and since turbulent flow regimes are exceptional, there is a preference for using the Carman–Kozeny drag relation. Kozeny proposed a fixed pore shape factor $K = 180$ in Eq. (1) to fit the model results to experimental data. In the literature, many other values are proposed (Ozgumus et al., 2014; Erdim et al., 2015; Hoyland, 2017; Schulz et al., 2019), of which $K = 150$ is also often used (Burke and Plummer, 1928; Ergun, 1952; Kramer et al., 2020a). The factor 180 does not appear to be constant at higher velocities when the flow is no longer laminar ($Re_\varepsilon > 2$), as Carman (1937) showed. He introduced a drag coefficient, which can be written in the laminar form (f_L) or in the turbulent form (f_T) as a function of the Reynolds number Re_ε:

$$f_L = f_T \; Re_\varepsilon = 180 + 2.9 \; {Re_\varepsilon}^{0.9} \qquad (Re_\varepsilon < 600) \tag{2}$$

Where f_L is the dimensionless drag coefficient (laminar representation) and f_T the dimensionless drag coefficient (turbulent representation) and where the modified particle Reynolds number Re_ε is defined as:

$$Re_\varepsilon = \frac{\rho_f d_p v_s}{\eta} \frac{1}{1-\varepsilon} \tag{3}$$

Where ρ_f is the fluid density. The experimentally obtained relation for f_L or f_T will be indicated below as the Carman drag coefficient (Carman, 1937). For further background information on the many forms of this equation, reference is made to the literature (Erdim et al., 2015) and model derivations given in the Supplementary Material (Section 3).

2.2. Particle correction shape factors

Within hydraulic modelling, particles are often idealised to spheres for mathematical convenience. Water treatment-related particles generally have more complex geometric features, summarised under the term shape, including the geometric shape, the presence of surface disparities such as protuberances and reentrant features as well as particle property irregularities. Shape is therefore difficult to define. Although the literature on particle shape is extensive (Gauvin and Katta, 1973; Holdich, 2002; Seville and Yu, 2016) and a number of shape factors and descriptors have been proposed (Clift et al., 1978; Allen, 1990), there is no universal agreement on how to define particle shape. Therefore, there is no agreement on how to correctly measure it, nor does the literature provide consistent methods to cope with naturally irregularly shaped particles that can be used in voidage prediction models for liquid-solid fluidisation systems. The size and shape of the particles has important implications for, for instance, filter design (Crittenden et al., 2012), but there is no easy way to account for this.

In the literature (Wadell, 1933; Cleasby et al., 1981; Michaelide et al., 2017) particle shape is often characterised by sphericity, which is generally defined as the ratio of the surface area of an equal volume sphere to the surface area of the granule. That being said, sphericity has limited value in actual practice for several reasons. First, filter media are currently still routinely measured and specified using a laborious sieve analysis procedure, and less by means of advanced image analysis techniques. Second, in the literature there is no general consensus on how to apply sphericity for commercially available granular media. If the particle has a known geometric shape, sphericity can be calculated mathematically. However, for irregularly shaped particles, indirect methods are required. To determine shape factors, several empirical fitting models are available (Dharmarajah, 1982). Often, these models are based on head loss or voidage experiments. Carman (1937) proposed that the K-value was independent of media properties and introduced a correction factor to account for the non-spherical nature of filter grains, using sphericity and the shape factor (Fair et al., 1933). According to Yang (2003), shape factors are open to criticism, because a range of granules with different shapes may have the same shape factor, which is inevitable if complex shapes are to be described by only a single parameter. Wen and Yu (1966) proposed shape factor corrections, used in the Ergun equation, based on experimental data for the minimum fluidisation voidage. According to the literature (Dharmarajah, 1982; Crittenden et al., 2012), a commonly used particle shape factor in fixed bed state is necessary in order to match the Carman–Kozeny predicted drag coefficient with the experimentally obtained drag coefficient. The main drawback of this approach is that the model parameters often have no direct connection to the underlying porous medium structure (Schulz et al., 2019), do not have a physical interpretation, or are difficult or even impossible to measure, especially by means of sieve analysis (di Felice, 1995).

In contrast, in the fluidised state, particle shape factors are usually omitted to match the Carman–Kozeny predicted drag coefficient with the experimentally obtained drag coefficient, without providing any explanation. Most likely this is done because these parameters are difficult to measure directly (de Jong and Nomden, 1974; Hoyland, 2017; Hunce et al., 2018). This is remarkable at the very least since the same particles are involved, in fixed as well as fluidised states. In addition, particle shape factors as a function of fluid velocity and temperature in liquid-solid fluidised systems are rarely evaluated in the literature. In the practice of filtration (Crittenden et al., 2012) and other forms of flow through granular beds, the measured resistance does not appear to correspond with the calculated resistance. To obtain a fit, an experimentally determined shape factor ϕ_s is used to modify the measured diameter (d) into an effective diameter (d_p):

$$d_p = \phi_s \; d \tag{4}$$

Where d is the measured diameter and ϕ_s the diameter shape correction factor. For further background information on the manifold empirical adjustments for flow resistance, reference is made to the literature (Říha et al., 2018).

3. Research aims

Based on theoretical factors and the specific ETSW procedure as applied after filter backwashing, it is clear that in order to obtain a thorough understanding of the hydraulics of up-flow filtration systems applied in full-scale water treatment unit operation, several goals must be met. Initially, a more effective drag coefficient must be introduced to be able to visualise changes in drag for various velocities and temperatures. The magnitudes of particle correction shape factors must be shown in fixed and fluidised state. To demonstrate the degree of irregularity of considered

Table 1
ImageJ morphological properties (Ferreira and Rasband, 2012).

Property	Meaning
Aspect ratio	The width to height ratio of an elongated particle
Ferret diameter	Distance between two parallel tangents on opposite sides of the image of a randomly oriented particle
Circularity	Perimeter of sphere of the same projected area divided by the actual projected perimeter of the particle
Solidity	The area of a particle divided by its convex hull area; the imaginary convex hull around it

granular material as well as to determine preferred particle orientation, an applicable image analysis method must be developed. In addition, a hydraulic explanation must be offered for the effective ETSW method for future optimisation purposes (water throughput and operational time) and to improve water quality.

4. Materials and methods

4.1. Particle selection and physical properties

For up-flow filtration and fluidisation experiments, rapid filtration sand grains were selected. The particle density was determined using measured differential pressures and a laboratory pycnometer. The hydraulic equivalent particle diameter (Dallavalle, 1948; Crittenden et al., 2012; Davis, 2010) was calculated using the sieve diameters, expressed in Eq. (5):

$$d_p = \sqrt{d_{s,1}\ d_{s,2}} \tag{5}$$

Where $d_{s,i}$ is the sieve mesh diameter. The dimensions of the particles were also determined by using ImageJ as a particle analyser (Ferreira and Rasband, 2012), for which a 4.188 g sample of filter sand was scanned on an A4 flatbed scanner, at a resolution of 2400 dpi. Irregularly shaped particles, in particular elongated parts, tend to lie horizontally oriented. ImageJ determines for each individual particle which pixel in the 2D-image belongs to this particle. For each particle, the software determines some 34 size parameters, such as equivalent circle diameter, and equivalent ellipse dimensions with related morphological particle properties (Table 1), such as aspect ratio, Ferret diameter, circularity and solidity. Statistical information such as mean, range and frequency distribution can be determined from all these measurements.

The total mass and measured density were used to calculate the total volume of the particles. Assuming an ellipsoid based on length and width of the average of the 2D dimensions gives a pseudo-3D height as average value for all particles.

4.2. Hydraulic experimental set-up

Filtration and expansion experiments were carried out at three locations: in Waternet's Weesperkarspel drinking water pilot plant located in Amsterdam, the Netherlands; at the University of Applied Sciences Utrecht, the Netherlands; and at Queen Mary University of London, United Kingdom. In all experiments, locally produced drinking water was used. The set-up (Fig. 1) consisted of a 4 m high transparent PVC pipe with an inner diameter of 57 mm. Water temperature was regulated with a boiler, a cooler and a thermostat by recirculating water through a buffer vessel connected to a water reservoir. An overflow at the top of the reactor returned water to the buffer vessel. From the buffer vessel, water was pumped through the reservoir connected to the thermostat which was set to a programmed water temperature.

Through filtration and expansion experiments, bed voidage and pressure drop were measured as a function of various linear fluid flow rates and temperatures. Hydraulic experiments were started in fixed bed state, obtained after an initial backwash with full fluidisation, which resembled the typical practical conditions of rapid sand and multimedia filters. By increasing the flow rate, the bed height was carefully observed and measured to determine any change in bed height and consequently average voidage. By measuring the differential pressure, the flow rate of the incipient fluidisation point was detected. By further increasing the flow rate, a sequence of bed voidages and differential pressures was measured to be able to compose an expansion curve. Based on acquired bed voidage, differential pressure, superficial fluid velocity, particle size and kinematic fluid viscosity, the drag coefficients were determined as presented in Section 2.1.

Photographs of particles, technical information about experimental set-up devices and operational procedures can be found in the Supplementary Material (Sections 1 and 2).

4.3. Dynamic shape factor determination

To investigate the variability of the particle shape factor, the ratio of the measured drag coefficient f_L and the drag coefficient for Carman–Kozeny $f_{L,CK}$, using Eq. (2), was calculated. We hypothesised that this ratio would depend on the hydraulic state, i.e. on the ratio $Re_\varepsilon/Re_{\varepsilon,mf}$ of the actual modified particle Reynolds number (Eq. (3)) and that for incipient fluidisation. Inverting the Carman–Kozeny equation, for the measured voidage, velocity and viscosity, it was possible to estimate the average particle size. Accordingly, a *dynamic* shape factor could be determined for various flow rates using a numerical solving method based on Bolzano's numerical intermediate value theorem. This is a straightforward solving method described in: (Apostol, 1967). A simplified equation states:

$$\phi_s = \sqrt{\frac{f_{L,CK}}{f_L}} \tag{6}$$

Where $f_{L,CK}$ is the dimensionless drag coefficient (laminar representation for Carman–Kozeny).

5. Results and discussion

5.1. Particle properties

Samples of RSF granules were obtained from a full-scale RSF unit operation located at the Waternet facility in Loenderveen, the Netherlands. The applied filter sand range (see Fig. 2) was obtained by using sieves of 0.80 and 1.25 mm. This was confirmed by sieving with 10 sieves between 0.6–2.8 mm (NEN-EN 933–2, n.d.), showing that 10 wt-% of the particles were smaller and 1 wt-% were larger than this range, which corresponds to a respective 20% and 1% in terms of the number of particles. We measured an average particle diameter of d_{50} = 0.90 mm based on particle counting.

The full-colour scan obtained from the A4 flatbed scanner was initially converted into a single-colour picture for maximum particle distinction from which a binary (black and white) picture was created with a pixel size of around 0.01 mm (2400 dpi). The size of each (black) particle was measured through pixel counting. Observed particles with their particle numbers can be shown as outlines on top of the original scan (see Fig. 3). The 4.188 g sam-

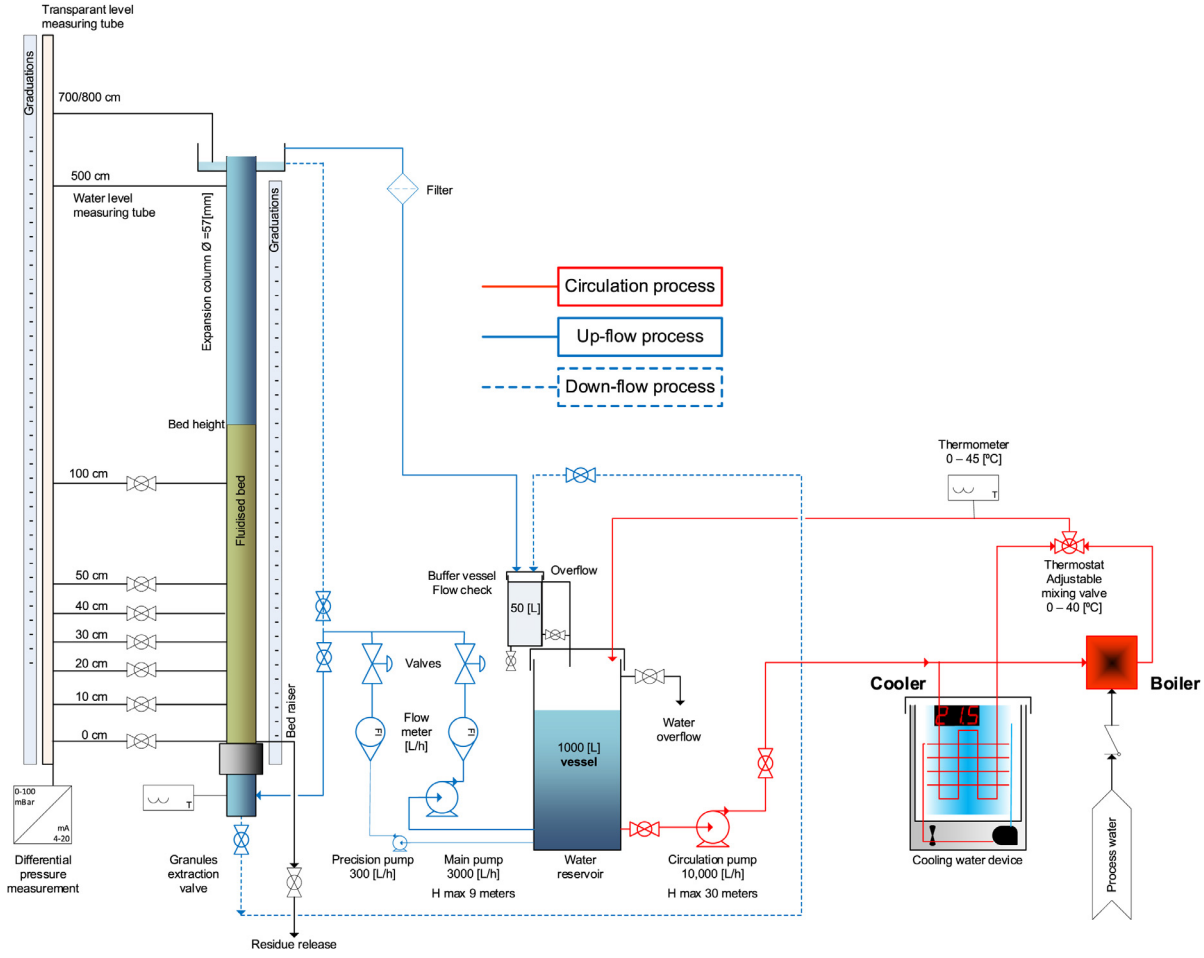


Fig. 1. Schematic overview of experimental set-up in all experimental locations.

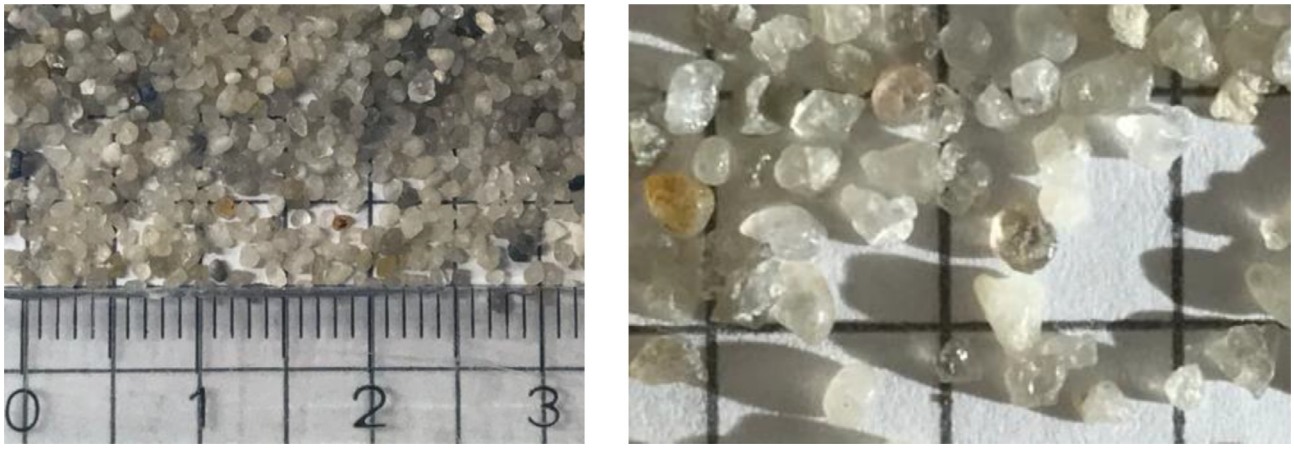


Fig. 2. Rapid sand filter granules 0.8 < d_p < 1.25 mm.

ple contained 2040 particles, each analysed by its size, shape and other morphological properties in ImageJ.

Figs. 4 and 5 show the measured distribution and cumulative frequency, respectively, of observed equivalent particle diameter. The green areas indicate the specification of the filter material based on information from the supplier of the two sieves (bottom sieve and top sieve). The projected area per particle, determined with ImageJ, was used to obtain the equivalent diameter of a circle resembling the basics of square sieve grids, as illustrated in Fig. 4. Giving the exact contours per particle allows for the calculation of an equivalent ellipse with the same area for each particle, giving two independent diameters d_{50} of 1.57 and 1.21 mm on average, with an aspect ratio of 1.30. Assuming that an ellipsoid with these two axes has the same volume as the average particle gives the third diameter of 0.78 mm. This dimension explains the sieve passage as particles are passing sieves in an upright orientation, contrary to the scanned particles lying in a horizontal orientation.

Fig. 5 illustrates how smaller particles are obtained which did not pass through the lowest sieve with the smallest mesh size,

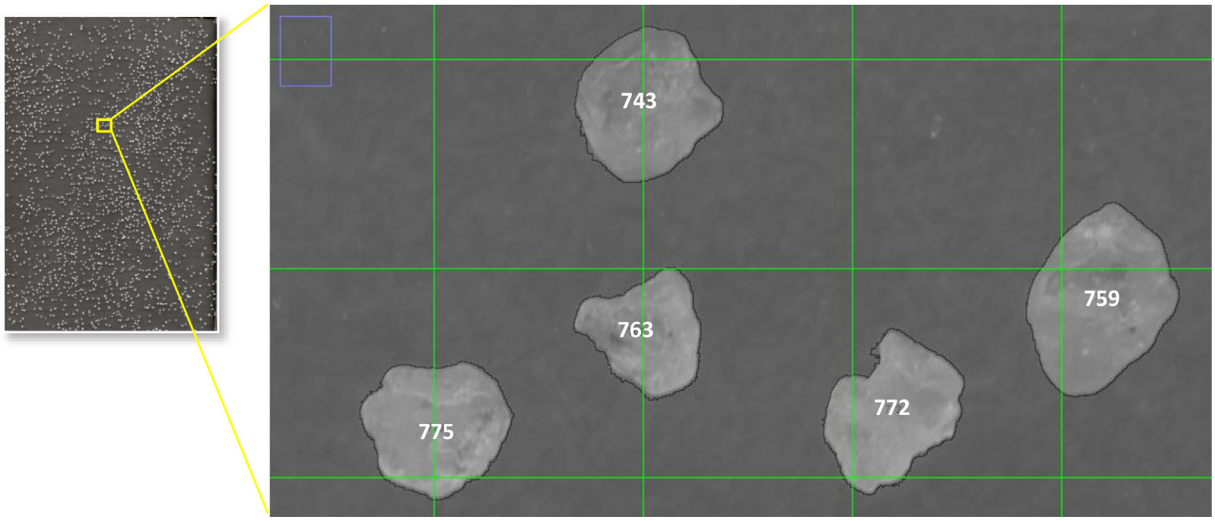


Fig. 3. Scanned sample with particle analysis with ImageJ, with particle outlines and particle numbers, with 2 × 2 mm gridlines.

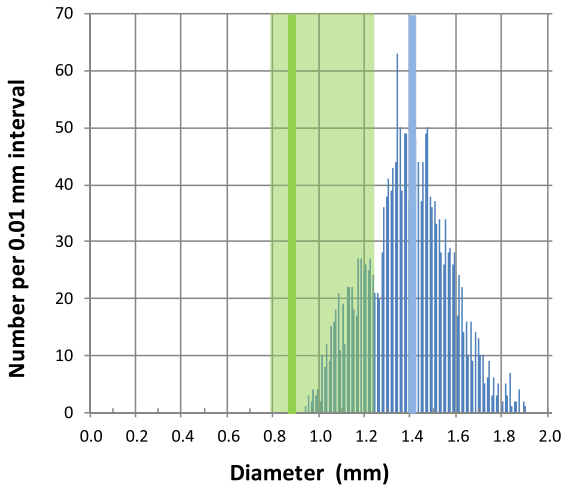


Fig. 4. Equivalent diameter (assumed to be a circle): histogram of circle diameter from particle areas of ImageJ (in blue), compared to filter sand specifications (green area). The average diameters based on particle counting (d_{50}) are presented as vertical lines in green (sieve experiment) and blue (ImageJ), respectively. (For interpretation of the references to colour in this figure legend, the reader is referred to the web version of this article.)

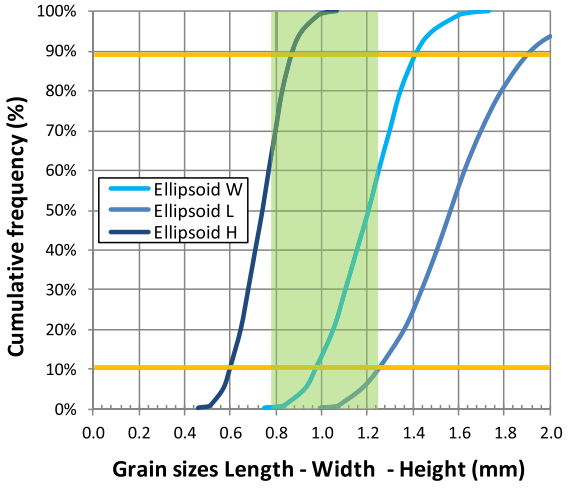


Fig. 5. Cumulative frequency grain sizes.

Table 2
Particle properties rapid filtration sand grains.

Variable	RSF grains	Unit
Particle sieve sizes	0.80–1.25	[mm]
Particle density	2638 ± 11	[kg/m^3]
Equivalent circle diameter 2D (average) [2)]	1.38	[mm]
Uniformity 2D (d_{60}/d_{10}) [2)]	1.26	[-]
Circularity 2D (average) [2)]	0.73	[mm]
Ellipsoid 3D-d50 [2)]	1.57 • 1.21 • 0.78	[mm]
Ellipsoid aspect ratios 3D - l/b-b/h [2)]	1.30 - 1.55	[-]
Geldarts type [3)]	D	

[1]Measured particle size distributions are given in the Supplementary Material (Section 4).
[2] ImageJ (Ferreira and Rasband, 2012).
[3] Geldarts particle classification (Geldart, 1973) type D: spoutable particles.

probably as a result of short sieving time. In contrast, hardly any larger particles were found since they did not pass through the top sieve with the largest mesh size. Fig. 5 also shows that the particles are not perfect spheres, as a sieve curve would suggest, but that they are much better described as an ellipsoid with three distinct dimensions: width, height and length.

In sum, it can be concluded that the analysed RSF grains are moderately irregularly shaped, and far from spherical. In the next section, it will become clear why this information is important in relation to decreasing bed resistance for increasing flow rates. Particle analysis using flatbed scans with pseudo-3D image processing is superior to 1D sieve analyses. The determined particle properties of RSF grains are presented in Table 2.

In industrial practice, samples of granules are still commonly sieved to obtain information about the particle size distribution for process monitoring. With this method, the morphological properties of the particles are lost. However, as irregularly shaped particles, and rod-like particles in particular, can realign and pass to lower sieves, this gives a distorted view of the actual particle sizes. The easily acquired particle information, i.e. average particle size, is entered accordingly into the drag coefficient or voidage prediction model. In practice, this classical method works well for spherical particles, but it is less accurate for irregularly shaped particles such as RSF grains (Fig. 2). Irregularly shaped particles experience anisotropic drag in fixed and fluidised state, due to the surrounding fluid and interactions with adjacent particles and the wall (Mahajan et al., 2018).

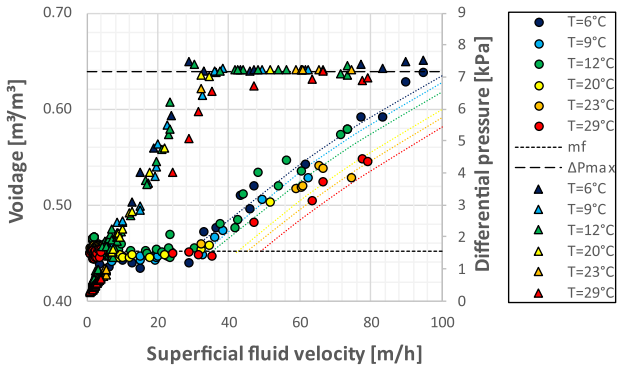


Fig. 6. Up-flow filtration and expansion curve for rapid filter sand granules 0.8 < d_p < 1.25 mm. Experimental voidage (circles), Carman–Kozeny predicted voidage (•••) and differential pressure (triangles) against superficial fluid velocity, (- - -) maximum pressure drop, (—) voidage at minimum fluidisation.

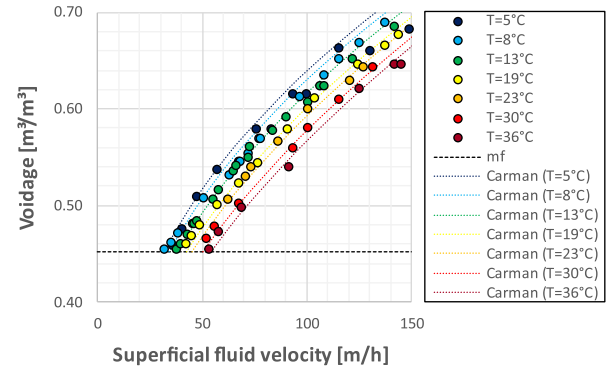


Fig. 7. Fluidisation characteristics of rapid filter sand granules 0.8 < d_p < 1.25 mm. Experimental voidage (circles) and Carman–Kozeny predicted voidage (•••) against superficial fluid velocity for six different water temperatures.

5.2. Hydraulic experiments and expansion curves

The hydraulic experiments we conducted provided crucial information about differential pressure and bed height in fixed, incipient and fluidised states, as a function of linear flow rates and water temperatures. In total, eight up-flow experiments were conducted for RSF grains at six different water temperatures (6–29 °C). Additional expansion experiments were performed at seven different water temperatures (5–36 °C) to determine the minimum or incipient fluidisation points, causing the first particles to expand as well as allowing the precise expansion behaviour of RSF grains to be determined. For up-flow filtration, the fluid flow was gradually increased until the incipient fluidisation point was reached, where the differential pressure levelled at a maximum value. For moderate fluidised state, the fluid flow was slightly further increased under constant maximum differential pressure. The expansion curve for RSF grains is presented in Fig. 6 The measured voidage in fixed bed state varies between $\varepsilon_0 = 0.44 \pm 0.03$. The voidage at the minimum fluidisation velocity is $\varepsilon_{mf} = 0.45 \pm 0.01$. Fig. 6 shows the expansion behaviour of RSF grains in the fluidised state. The measured bed voidages at various water temperatures agree reasonably well with the predicted values according to the Carman–Kozeny model. The influence of the water temperature in the fluidised state can be seen in Fig. 7. The temperature effect in the fixed bed state was less clearly observable (Fig. 6). A moderate linear relationship ($R^2 = 0.99$) between the degree of subsidence% of the packed bed and water temperature (5–35 °C) was found: $\Delta\varepsilon/\varepsilon = -0.0001T + 0.008$. The temperature dependence of the bed setting is caused by the changes in viscosity of water, which affects the frictional forces acting on the filter bed.

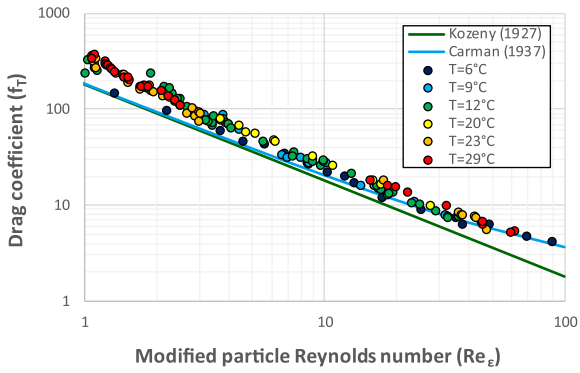


Fig. 8. Drag (turbulent representation) f_T against modified Reynolds number for rapid filter sand granules 0.8 < d_p < 1.25 mm.

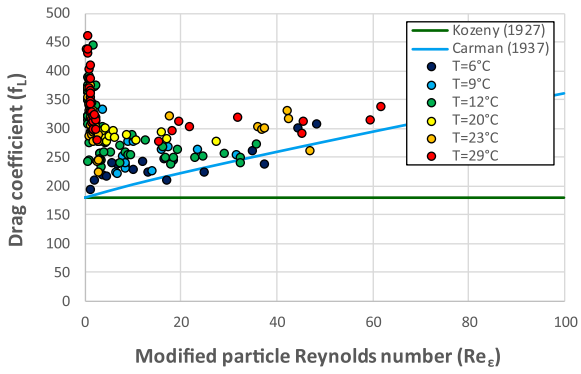


Fig. 9. Drag (laminar representation) f_L against modified Reynolds number for rapid filter sand granules 0.8 < d_p < 1.25 mm.

Experimental data tabulation (Section 9), minimum fluidisation points (Section 5) and model predictions (Section 3) are given in the Supplementary Material.

5.3. Measured and predicted drag coefficients

The drag coefficient against the modified Reynolds number Re_ε for RSF grains is presented in turbulent representation f_T in Fig. 8 and in laminar representation f_L in Fig. 9. In both figures, the Kozeny and Carman (Eq. (2)) drag relations are plotted. Fig. 8 shows a clear deviation between the measured and predicted values for low Reynolds numbers ($Re_\varepsilon < 10$). In most other literature references (Burke and Plummer, 1928; Carman, 1937; Ergun, 1952; Gibilaro, 2001; Bird et al., 2007; Hoyland, 2017), such deviations between measurements and drag models are artificially hidden by the use of logarithmic scales over several orders of magnitude.

For relatively high Reynolds numbers ($Re_\varepsilon > 10$), the predicted Carman values coincide relatively well with the measured values. For low Reynolds numbers (especially $Re_\varepsilon < 5$), the measured f_L values are significantly larger than the theoretically expected f_L =180, corresponding to the Kozeny pore shape factor $K = 180$. The laminar representation of f_L makes changes in drag much more concise compared to the commonly used turbulent representation of f_T. Fig. 9 clearly shows that the drag decreases considerably in case the fluid flow increases slightly, under laminar or transitional conditions. This is happening while the particles are still assumed to be packed in the fixed bed state.

More information about the Carman model can be found in the Supplementary Material (Sections 3).

To show explicitly that the drag decreases mainly in the (supposedly) fixed bed, the ratio of measured to predicted drag $f_L/f_{L,CK}$

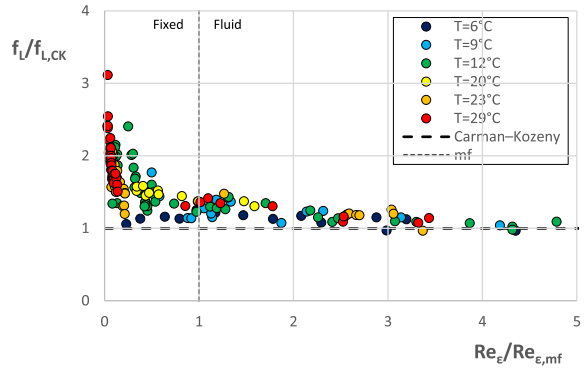


Fig. 10. Drag (laminar representation) relative to the Carman–Kozeny drag against modified Reynolds numbers relative to modified Reynolds numbers at minimum fluidisation for rapid filter sand granules 0.8 < d_p < 1.25 mm.

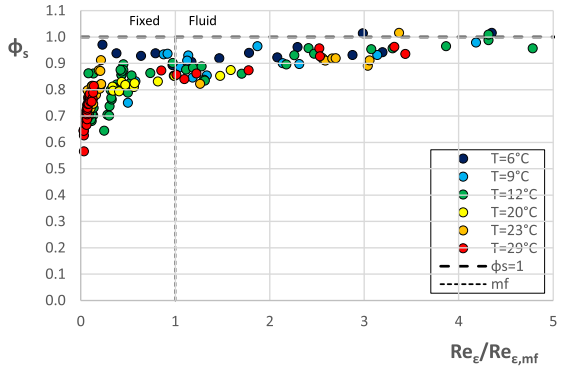


Fig. 11. Shape factor against modified Reynolds numbers relative to modified Reynolds numbers at minimum fluidisation for rapid filter sand granules 0.8 < d_p < 1.25 mm.

is plotted against the Reynolds number ratio $Re_\varepsilon/Re_{\varepsilon,mf}$ in Fig. 10. For increasing flow rates, where $Re_\varepsilon/Re_{\varepsilon,mf}$ is still well below 1, the ratio $f_L/f_{L,CK}$ decreases rapidly. For every percent that the bed voidage drops, the drag coefficient f_L decreases by a factor 4. The large ratio of measured to predicted drag occurs at $Re_\varepsilon/Re_{\varepsilon,mf}$ < 0.5, which indicates that it cannot be explained by effects occurring around v_{mf}. This will be investigated further in the next subsection.

A practical approach is to use a particle shape factor to compensate for observed deviations in f_L. The use of a shape factor, however, becomes redundant in the fluidised state, since the prediction of the voidage is increasingly consistent with the models for (Re_ε > 10) in Figs. 9 and 10. We reiterate that the common use of two different shape factors in the literature for fixed beds (Ergun, 1952; Yang, 2003; Li et al., 2018) and fluidised beds (di Felice, 1995; Gibilaro, 2001; Rhodes, 2008) is remarkable, because it concerns the same particles. Using Eq. (6), shape factors were calculated for RSF grains. Fig. 11 shows that in the fixed bed state, the particle shape factor varies between approximately 0.6 < ϕ_s < 0.9. In the fluidised state, however, the shape factor slowly approaches $\phi_s = 1$.

5.4. Hydraulic explanation for up-flow filtration and ETSW

When a fluid flows in upward direction through a particle bed in fixed state, the fluid exerts a certain drag on the particles. The transition from a fixed bed to a fluidised bed occurs when the pressure drop across a packed bed reaches a constant maximum value, after the fluid flow exceeds the minimum fluidisation velocity. The particles start to elevate, and irregularly shaped particles also show changing orientation, realignment and rearrangement in their packing position. During the pilot plant experiments, the observed bed height decreased slightly (approximately 1%), which can be seen in Fig. 12, Figs. 13 and 14. Videos of RSF grains (Kramer and van Schaik, 2020) as well as calcite pellets (Kramer et al., 2020b), at flow rates well below the minimum fluidisation points, show clearly that particles already start to move locally while overall they remain in a fixed bed state. The collapse of the packed bed caused by ETSW is also demonstrated in four videos.

The collapse of the particles in the fixed beds below the incipient fluidisation point is most likely caused by particle orientation, realignment and rearrangement in their packing position. An unsteady packed bed in moderate up-flow conditions is pseudo-fixed and in a setting state. This results in a decreasing bed voidage and simultaneously in a decreasing drag coefficient, which seems quite contradictory. However, this can be explained by the collapse of



Fig. 12. Initial fixed bed.



Fig. 13. Fixed bed setting after t=5 [min] ETSW.



Fig. 14. Fixed bed setting after t=30 [min] ETSW.

local channels (Figs. 15b and c) in the bed, leading to a more uniform flow distribution through the bed and improving the available surface for flow-through (Hassett, 1961). This is the reason why ETSW, as an additional method to a backwash filter recipe, works effectively (Fig. 15), since it levels the voidage in the particle bed. In this way, the successful ETSW method proposed by Amburgey (2005) can be explained.

During full-scale operational ETSW procedures, small (1–10 mm) spouting channels were observed: this is shown in Fig. 15(b) and Fig. 15(c). The amount and intensity of spouts decreased during the procedure. A plausible explanation is that the up-flow filtration caused the channels to collapse in the bed, leading to a more uniform flow distribution through the bed and improving the available surface for flow-through. We hypothesise that this phenomenon has a positive effect on water quality, since the magnitude of turbidity and particle count spikes decrease. Therefore, the successful optimisation ETSW filter backwashing procedure proposed by Amburgey (2005) can be explained hydraulically.

5.5. Preliminary considerations of hydraulics-based ETSW

According to Amburgey (2005), adjustments in fluid velocity should be limited to the minimal fluidisation velocity. Since this velocity depends on both the filter bed material and on water temperature, optimising the up-flow velocity could become complicated due to different packing materials and seasonal temperature fluctuations. Smaller RSF grains fluidise more easily compared to the larger RSF grains, resulting in a gradual transition. In other words, because of differences in particle size, the minimum fluidisation velocity cannot be determined exactly. In the event that during ETSW velocities occur that are too high, the benefits of bed setting, a more uniform flow distribution throughout the bed and better available surface for through-flow are nullified. Therefore, when optimising the ETSW time, it may be more important to focus on effective bed subsidence instead of focussing on incipient fluidisation. Amburgey (2005) assumed that at least one bed volume would be required to wash out remaining particles. As we provide a hydraulic explanation for improved water quality, this assumption does not need to apply. Therefore, considering this hydraulic explanation, the ETSW time could potentially be shortened to less than one bed volume. This would decrease down-time due to backwashing and increase up-time (filtration time) as breakthrough at restart will be significantly reduced, or even eliminated. With regard to water quality and costs, the elimination of breakthrough at restart will improve the overall bulk quality of the produced water, increase the total volume produced in between backwashes and subsequently save overall production costs. In practice, the first half hour of filtration, after backwashing, is discarded as this contains the highest concentrations of remaining particulates and contamination.

5.6. Full-scale consequences of utilising the ETSW procedure

Turbidity is a measure of the amount of particulate matter in water and is one of the most widely used parameters for mea-



(a) *Full-scale RSF during collapse pulsing 40 m/h backwashing scour*



(b) *Full-scale RSF during ETSW 5 m/h up-flow* ***(c)*** *Full-scale RSF during ETSW bed, spouting channels*

Fig. 15. (a) Full-scale RSF during collapse pulsing 40 m/h backwashing scour; (b) Full-scale RSF during ETSW 5 m/h up-flow; (c) Full-scale RSF during ETSW bed, spouting channels.

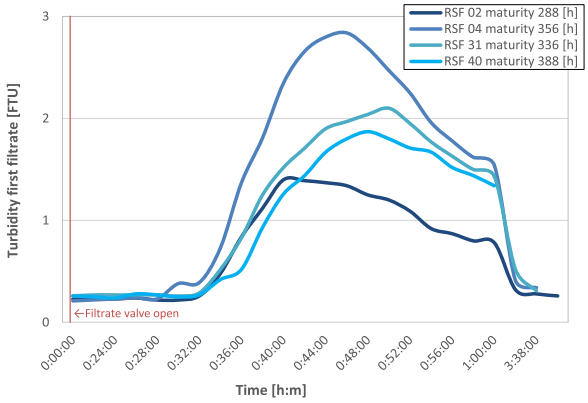


Fig. 16. Turbidity measurements of four full-scale RSF first filtrates in Loenderveen before the ETSW procedure was established.

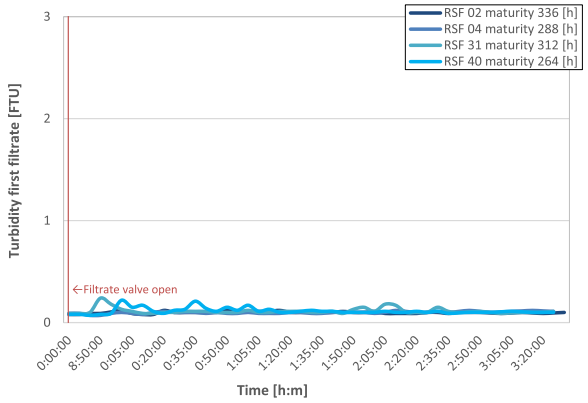


Fig. 17. Turbidity measurements of four full-scale RSF first filtrates in Loenderveen after the ETSW procedure was established.

suring water quality prior to disinfection (Edzwald, 2011). High turbidity levels can reduce disinfection capacity. Adequate turbidity removal implies the partial removal of pathogens in water (Lechevallier et al., 1991), since most pathogens tend to aggregate with particles. Before 2016, at the full-scale RSF in Loenderveen (the Netherlands), considerable turbidity spikes were detected in the first filtrate after backwash cycles. After a backwash cycle had been completed and the filter returned to operational mode, the turbidity of the first filtrate was measured in four filters (Fig. 16). After approximately 30 min, the turbidity increased from 0.2 FTU up to 1–3 FTU. A similar elevated pattern could be seen for bacterial levels Enterococci (N=4/10 L), E.coli (N=14/10 L) and traces of sulphite-reducing Clostridia (N=10^3/10 L). The WHO (World Health Organization, 2017) promotes a turbidity threshold of below 0.2 NTU.

Accordingly, an optimisation process has been started at the full-scale facility in Loenderveen to improve water quality by reducing bacterial breakthroughs. The goal was to decrease the concentrations of bacteria to improve the oxidation and disinfection efficiency in the ozonation unit operation down-stream (van der Helm, 2007). The ETSW procedure was initialised on the full-scale facilities additional to the standard backwash procedure. Furthermore, we investigated whether it was desirable to remove the first filtrate for approximately three hours. After the ETSW procedure was utilised, turbidity spikes in the first filtrates were excluded (Fig. 17) in favour of water quality.

6. Conclusions

Our experiments showed that irregularly shaped particles such as RSF grains in fixed beds under moderate up-flow conditions show non-monotonous hydraulic behaviour related to changing orientation, realignment and rearrangement in particle packing position. This happens in such a manner that the bed offers the maximum flow passage, i.e. voidage to the fluid. Initially, the bed voidage, the flow-through interface available in the bed, as well the drag decrease and accordingly increase for larger fluid flows. These phenomena also affect the volume-based voidage prediction, something that to the best of our knowledge has not been elucidated in the literature.

In the field of engineering, a shape factor is applied to compensate for the above aspect in the fixed and incipient fluidisation but is omitted when the fluidised state is described. In this research, it was shown that such a shape factor is not a constant particle property but is dependent on the fluid properties as well. This dynamic shape factor for irregularly shaped RSF grains increases from approximately 0.6 until 1.0 in fairly fluidised state. The use of constant shape factors regarding natural, irregularly shaped granules is therefore not recommended. Our new straightforward image analysis method, based on a weighted particle sample to estimate the mean measures of spheroids, shows that sieve measures are not representative of natural, irregularly shaped granules. Based on experimental data obtained in this work, it is shown that, for increasing fluid flow rates, the fixed bed voidage decreases slightly (approximately 1%) while the drag coefficients decline to a considerable degree. The drag coefficient reached values up to 450 (in laminar representation), which is considerably larger than the well-known Kozeny value of 180.

The reduction in bed voidage as well as bed resistance is due to the realignment of the particles in the packed bed and the collapse of flow channels created during a normal backwash procedure. Particle orientation, realignment and rearrangement implies unstable fixed beds that become denser in laminar up-flow conditions. This results in a decreasing bed voidage and simultaneously in a decreasing drag coefficient. A complete fluidised state, i.e. exceeding the minimum fluidisation velocity, is not necessary. In addition, besides the particle size, also the particle shape is a decisive factor in the phenomena occurring in the particle beds. The collapse of local channels in the bed leads to a more uniform flow distribution through the bed and improves the available surface for flow-through. In this way, the successful ETSW method proposed by Amburgey (2005) can be explained.

7. Recommendations

With the knowledge acquired during these experiments, the ETSW procedure can, in future research, be further optimised by adjustments to the up-flow velocity and time.

During our experiments, it was possible to capture the almost unnoticeable changes in the particle bed on video. In a full-scale installation, real-time monitoring of the particle collapse in the rapid sand filter bed is practically impossible. Thorough pilot plant research is required to fully understand the specific processes of a particular water treatment. Every water treatment plant has a different context i.e. water quality (load of particulate material), bed composition, different process strategies and different water temperatures.

Since the configuration of the particles in the packed filter bed is generated by frictional forces, it is recommended to investigate alternative methods that include frictional forces, so that subsidence can take place. Although filter resting could also be a solution to acquire bed setting and prevent the first filtrate turbidity spike after the backwash expansion, it reduces the operational up-

time. In order to extend the hydraulic impact discussed here to an even more effective ETSW, a model to predict the permeability and bed setting of the filter bed needs to be further substantiated and developed to be able to optimise the ETSW procedure. The newly proposed pseudo-3D ImageJ analysis method can be used for future CFD modelling research, taking into account the influence of non-spherical particles, in which the obtained measures of the ellipsoids can be put to good use.

Declaration of Competing Interest

The authors declare that they have no known conflicts of interests or personal relationships that could have appeared to influence the work reported in this article.

Acknowledgements

This research is part of the project “Hydraulic modelling of liquid-solid fluidisation in drinking water treatment processes” carried out by Waternet (the water utility of Amsterdam and surroundings), Delft University of Technology and HU University of Applied Sciences Utrecht. Financial support came from Waternet’s Drinking Water Production Department.

We acknowledge and thank our students from Delft University of Technology, HU University of Applied Sciences Utrecht and Queen Mary University of London and in particular Victor Shao and Cas van Schaik for the precise execution of many laboratory and pilot plant experiments.

This research project did not receive any specific grant from funding agencies in the public, commercial or not-for-profit sectors.

Supplementary materials

Supplementary material associated with this article can be found, in the online version, at doi:10.1016/j.watres.2021.117085.

References

Allen, T., 1990. Particle Size Measurement–Powder Technology Series, 4th ed. Chapman and Hall, London doi:10.1007/978-94-009-0417-0.

Amburgey, J.E., 2005. Optimization of the extended terminal subfluidization wash (ETSW) filter backwashing procedure. Water Res. 39, 314–330. doi:10.1016/j.watres.2004.09.020.

Amburgey, J.E., Amirtharajah, A., 2005. Practical and theoretical guidelines for implementing the extended terminal subfluidization wash (ETSW) backwashing procedure. J. Water Supp.: Res. Technol.-Aqua 54, 329–337. doi:10.2166/aqua.2005.0031.

Apostol, T.M., 1967. One-Variable Calculus, with an Introduction to Linear Algebra, 2nd ed. John Wiley & Sons, Inc., New York.

Bird, R.B., Stewart, W.E., Lightfoot, E.N., 2007. Transport Phenomena, Revised, 2nd ed. John Wiley & Sons, Inc. International, New-York.

Blake, F.C., 1922. The resistance of packing to fluid flow. Trans.Am. Inst. Chem. Eng. 14, 415–421.

Burke, S.P., Plummer, W.B., 1928. Suspension of macroscopic particles in a turbulent gas stream. Ind. Eng. Chem. 20, 1200–1204. doi:10.1021/ie50227a026.

Camp, T.R., 1946. Sedimentation and the design of settling tanks. Trans. Am. Soc. Civil Eng. 111, 895–936.

Carman, P.C., 1937. Fluid flow through granular beds. Trans., Inst. Chem. Eng. 15, 32–48. doi:10.1016/S0263-8762(97)80003-2.

Cleasby, J.L., Asce, M., Fan, K.S., 1981. Predicting fluidization and expansion of filter media. J. Environ. Eng. Division 107, 455–471.

Clift, R., Grace, J.R., Weber, M.E., 1978. Bubbles, Drops, and Particles. Academic Press., San Diego, San Diego, C.A.

Crittenden, J.C., Trussell, R.R., Hand, D.W., Howe, K.J., Tchobanoglous, G., 2012. MWH’s Water Treatment: Principles and Design, 3rd ed. John Wiley & Sons, New York.

Dallavalle, J.M., 1948. Micromeritics–the Technology of Fine Particles, 2nd ed. Pitman Publishing Ltd, London.

Darcy, H., 1856. Les fontaines publiques de la ville de Dijon: Exposition et application des principes a suivre et des formules a employer dans les questions de distribution d’eau; ouvrage terminé par un appendice relatif aux fournitures d’eau de plusieurs villes au filtr. Victor Dalmont. Libraire Des Corps imperiaux Des Ponts Et Chaussées Et Des Mines. Dijon.

Davis, M., 2010. Water and Wastewater Engineering–Design principles and Practice, 1st ed. McGraw-Hill, New-York.

de Jong, J.A.H, Nomden, J.F., 1974. Homogeneous gas-solid fluidization. Powder Technol. 9, 91–97.

Dharmarajah, A.H., 1982. Effect of Particle Shape on Prediction of Velocity-Voidage Relationship in Fluidized Solid-Liquid Systems. Ames.

di Felice, R., 1995. Review article number 47: of hydrodynamics of liquid fluidisation. Chem. Eng. Sci. 50, 1213–1245. doi:10.1016/0009-2509(95)98838-6.

Edzwald, J.K., 2011. Water quality and treatment: a handbook on drinking water. American Water Works Association, 6th ed. American Society of Civil Engineers, McGraw-Hill, New York.

Erdim, E., Akgiray, Ö., Demir, I., 2015. A revisit of pressure drop-flow rate correlations for packed beds of spheres. Powder Technol. 283, 488–504. doi:10.1016/j.powtec.2015.06.017.

Ergun, S., 1952. Fluid flow through packed columns. Chem. Eng. Sci. 48, 89–94.

Fair, G.M., Hatch, L.P., Hudson, H.E., 1933. Fundamental factors governing the streamline flow of water through sand. Jo (Amo Water Works Assoco) 25, 1551–1565. doi:10.1002/j.1551-8833.1933.tb18342.x.

Ferreira, T., Rasband, W., 2012. ImageJ user guide, ImageJ user guide IJ 1.46r. doi:10.1038/nmeth.2019.

Forchheimer, P., 1930. Hydraulik, 3rd ed. B.G. Teubner, Leipzig.

Gauvin, W.H., Katta, S., 1973. Momentum transfer through packed beds of various particles in the turbulent flow regime. AIChE J. 19, 775–783. doi:10.1002/aic.690190415.

Geldart, D., 1973. Types of gas fluidization. Powder Technol. 7, 285–292. doi:10.1016/0032-5910(73)80037-3.

Gibilaro, L.G., 2001. Fluidization-Dynamics, the Formulation and Applications of a Predictive Theory for the Fluidized State. Butterworth-Heinemann, Oxford.

Hassett, N.J., 1961. The mechanics of fluidization. Br. Chem. Eng. 19, 777–780.

Holdich, R.G., 2002. Fundamentals of Particle technology, Fundamentals of Particle Technology. Midland Information Technology and Publishing, Leicestershire doi:10.4236/ns.2010.210132.

Howe, K.J., Hand, D.W., Crittenden, J.C., Rhodes Trussell, R., Tchobanoglous, G., 2012. Principles of Water Treatment, 1st ed. John Wiley & Sons, Inc., New Jersey.

Hoyland, G., 2017. General combined model for the hydrodynamic behaviour of fixed and fluidised granular beds. Water Res. 111, 163–176. doi:10.1016/j.watres.2017.01.008.

Hunce, S.Y., Soyer, E., Akgiray, Ö., 2018. On the backwash expansion of graded filter media. Powder Technol. 333, 262–268. doi:10.1016/j.powtec.2018.04.032.

Kozeny, J., 1927. Über kapillare leitung des wassers im boden. Akad. Wiss.Wien 136, 271–306.

Kramer, O.J.I., Padding, J.T., van Vugt, W.H., de Moel, P.J., Baars, E.T., Boek, E.S., van der Hoek, J.P., 2020a. Improvement of voidage prediction in liquid-solid fluidized beds by inclusion of the Froude number in effective drag relations. Int. J. Multiphase Flow 127. doi:10.1016/j.ijmultiphaseflow.2020.103261.

Kramer, O.J.I., van Schaik, C., 2020. Videos of Up-Flow Filtration Velocities for Rapid Sand Filter Grains 0.8-1.25Mm in Water [Data set] 4TU.Centre for Research Data. 4TU.Centre for Research Data, The Netherlands doi:10.4121/13337057.v1.

Kramer, O.J.I., van Schaik, C., Nijssen, T.M.J., 2020b. Videos of Fluidisation of Calcite-Pellets 0.8-0.9mm and 1.4-1.7Mm in Water for Various Flow Rates [Data set] 4TU.Centre for Research Data. 4TU.ResearchData, The Netherlands doi:10.4121/13277246.v1.

Lechevallier, M.W., Norton, W.D., Lee, R.G., 1991. Occurrence of giardia and cryptosporidium spp. Surf. Water Suppl.. Appl. Environ. Microbiol. 57, 2610–2616. doi:10.1128/AEM.57.9.2610-2616.1991.

Li, X., Liu, M., Li, Y., 2018. Hydrodynamic behavior of liquid–solid micro-fluidized beds determined from bed expansion. Particuology 38, 103–112. doi:10.1016/j.partic.2017.08.002.

Mahajan, V.v., Nijssen, T.M.J., Kuipers, J.A.M., Padding, J.T., 2018. Non-spherical particles in a pseudo-2D fluidised bed: modelling study. Chem. Eng. Sci. 192, 1105–1123. doi:10.1016/j.ces.2018.08.041.

Michaelide, E., Crowe, C.T., Schwarzkopf, J.D., 2017. Multiphase Flow Handbook, 2nd ed. Taylor & Francis Inc, London.

Munson, B.R., Rothmayer, A.P., Okiishi, T.H., Huebsch, W.W., 2020. Fundamentals of Fluid Mechanics, 7th ed. John Wiley & Sons, New York.

NEN-EN 933-2, 2020. Tests for Geometrical Properties of Aggregates - Part 2: Determination of Particle Size Distribution - Test sieves, Nominal Sizes of Apertures, n.d.. Dutch norm ICS-code 91.100.15, 93.080.20.

Ozgumus, T., Mobedi, M., Ozkol, U., 2014. Determination of Kozeny constant based on porosity and pore to throat size ratio in porous medium with rectangular rods. Eng. Appl. Comput. Fluid Mech. 8, 308–318. doi:10.1080/19942060.2014.11015516.

Rhodes, M., 2008. Introduction to particle technology. Chemical Engineering and Processing, 2nd ed John Wiley & Sons Ltd., Chichester doi:10.1002/9780470727102.

Říha, J., Petrula, L., Hala, M., Alhasan, Z., 2018. Assessment of empirical formulae for determining the hydraulic conductivity of glass beads. J. Hydrol. Hydromech. 66, 337–347. doi:10.2478/johh-2018-0021.

Schulz, R., Ray, N., Zech, S., Rupp, A., Knabner, P., 2019. Beyond Kozeny–Carman: predicting the permeability in porous media. Transp. Porous Media 130, 487–512. doi:10.1007/s11242-019-01321-y.

Seville, J.P.K., Yu, C.Y., 2016. Particle Technology and engineering, an Engineer’s Guide to Particles and powders: Fundamentals and Computational Approaches, 1st ed. Butterworth-Heinemann.

van der Helm, A.W.C., 2007. Integrated Modeling of Ozonation for Optimization of Drinking Water Treatment. Water Management Academic Press, Delft.
Wadell, H., 1933. Sphericity and roundness of rock particles. J. Geol. 41, 310–331. doi:10.1086/624040.
Wen, C.Y., Yu, Y.H., 1966. A generalized method for predicting the minimum fluidization velocity. Am. Institu. Chem. Eng. J. 12, 610–612. doi:10.1002/aic.690120343.
World Health Organization, 2017. Guidelines for Drinking-Water Quality, 4th ed. World Health Organization.
Yang, W.C., 2003. Handbook of Fluidization and Fluid-Particle Systems, 1st ed. Chemical Engineering. CRC Press, New-York doi:10.1016/S1672-2515(07)60126-2.